Jordan Journal of Civil Engineering, Volume **15**, No. **2**, **2021**

A Simple Higher-order Shear Deformation Theory for Static Bending Analysis of Functionally Graded Beams

Hassina Ziou [1)*]***, Mohamed Guenfoud*** [2)] ***and Hamza Guenfoud*** [3)]

[1)] Senior Researcher, National Centre for Studies and Integrated Research on Building (CNERIB), Souidania, Algiers, Algeria.
* Corresponding Author. E-Mail: hassina.geniecivil@gmail.com
[2)] Professor, Department of Civil Engineering, University of Guelma, Algeria. E-Mail: gue2905m@yahoo.fr.
[3)] Doctor, Department of Civil Engineering, University of Guelma, Algeria. E-Mail: hamzaguenfoud@gmail.com

ABSTRACT

In this study, a polynomial higher-order shear deformation theory is introduced and developed for static analysis of functionally graded material (FGM) beams. The presented theory has strong similarities with Timoshenko beam theory in some aspects, such as equations of motion, boundary conditions and stress expressions. The developed theory does not require shear correction factor and satisfies the stress-free boundary conditions, such that the transverse shear stress varies parabolically through the beam thickness. The mechanical properties of the FGM beam are assumed to vary continuously in the thickness direction based on power-law distribution in terms of the volume fractions of the constituents. The influences of material distribution, boundary conditions, aspect ratio and neutral axis on the mid-plane deflection, normal stress and shear stress are figured out. The results obtained are compared with the data available in the literature to verify the correctness and the accuracy of the developed theory. The presented theory can provide a reference which other researchers can use for their studies.

KEYWORDS: Functionally graded material, Higher-order shear deformation theory, Finite element method, Power law, Neutral axis.

INTRODUCTION

Functionally graded materials (FGMs) are a class of composite materials the compositions of which can be changed according to the required performance. It can be produced with a continuously graded variation of volume fractions of constituents, which leads to a continuity of the material properties, which is the main difference between such a material and the usual composite one. FGMs are usually made of a mixture of ceramic and metals. The ceramic constituent of the material provides a high temperature resistance due to its low thermal conductivity, while the ductile metal constituent, on the other hand, prevents fracture caused by thermal stress. In other words, the metallic constituent is used to withstand the mechanical loads, while the ceramic one acts as thermal insulation.

A brief overview of recent works closely related to the current study is presented as follows: Kadoli et al. (2008) performed static analysis of beams made of metal-ceramic FGMs using a fined element based on a third-order shear deformation beam element. The material properties of the functionally graded beam are assumed to vary according to power-law function. Chakraborty and Gopalakrishnan (2003) investigated analytically static, free vibration and wave propagation of sandwich beams with a FGM core using the first-order shear deformation theory. Pindera and Dunn (1995) evaluated the higher-order theory by developing a detailed finite element analysis of the FGM. They found that the higher-order theory for functionally graded materials results agreed well with the finite element results. An exact element was developed by Ziou et al. (2016) to analyze the response of isotropic and FGM beam by a finite element method based on the first-order shear deformation theory. A beam theory similar to the Euler-Bernoulli beam theory for functionally graded beams was developed by Sankar

Received on 20/9/2020.
Accepted for Publication on 12/2/2021.

(2001). FGM beam with variation of volume fractions of ceramic and metal in the thickness direction based on exponential law was considered. A complete investigation on the significance of the transverse shear for the buckling analysis of FGM beam was performed by Ziou et al. (2020). Two separate finite element formulations were developed; one based on Euler-Bernoulli theory and the other one on Timoshenko beam theory. The results showed that the transverse shear should be considered to better predict the critical loads in FGM beam type structures. Bouazza et al. (2017) presented a new hyperbolic shear deformation theory to study the mechanical buckling analysis of FGM plates. The presented theory had only four unknown functions as against five in case of Mindlin-Reissner theory. Meksi et al. (2018) proposed a numerical procedure for the buckling analysis of FGM plates having parabolic-concave thickness variation. Thai and Vo (2012) experimented with high-order shear deformation theory to examine the vibration and bending responses of functionally graded beams. Nguyen et al. (2015) studied free vibration and buckling of sandwich beams using a high-order shear deformation theory. Thai and Vo (2012) used Sinusoidal Shear Deformation Beam Theory (SSDBT) to study bending, buckling and vibration behaviors of nanobeams. Vo et al. (2014) exploited the finite element method to study stability and vibration of a composite sandwich beam regarding a refined shear deformation theory. Rezaiee and Masoodi (2016) investigated exact natural frequencies and buckling load of functionally graded material-tapered beam-columns considering semi-rigid connections of the tapered beam-columns. The static behavior of non-prismatic sandwich beams composed of functionally graded FGM was investigated for the first time by Rezaiee-Pajand et al. (2018). Vo and Thai (2012) used refined beam theories to study the behavior of composite beams with arbitrary lay-ups and developed a two-noded C1 finite element with six degrees of freedom per node accounting for the shear deformation effects and anisotropy coupling. Ziou et al. (2020) proposed an efficient finite element formulation based on deformation approach for bending of functionally graded beams. The mechanical properties of the beam are assumed to vary continuously in the thickness direction by a simple power-law distribution in terms of the volume fractions of the constituents.

In the present work, an efficient higher-order shear deformation theory is developed to investigate the static behavior of functionally graded beams. The presented theory satisfies equilibrium conditions at the top and bottom faces of the beam without using shear correction factor. The material properties of FGM beams are assumed to vary through the thickness according to a power-law function. The impacts of material distribution, boundary conditions, aspect ratio and neutral axis on the bending behavior of FGM beam have been investigated. Numerical results are plotted and evaluated with the existing theories to verify the accuracy of the proposed theory.

Many higher-order shear deformation theories have been developed in the last decades. These theories can be chronologically classified as shown in Table 1.

MATHEMATICAL FORMULATIONS

Material Properties of FGM

Fig.1 illustrates a functionally graded beam of length L, width b and thickness h. The FGM beam is composed of two different materials: ceramic and metal. The effective material properties of the FGM beam, i.e., Young's modulus, Poisson ratio and shear modulus vary continuously and non-uniformly in the thickness direction according to power-law function. It can be expressed using the relation:

$$P(z) = P_c V_c + P_m (1 - V_c) \tag{1-a}$$

$$V_c = \left(\frac{1}{2} + \frac{z}{h}\right)^k \tag{1-b}$$

where P_c and P_m are the effective material properties of ceramics and metals, respectively.

V_c and V_m are the volume fractions of ceramic and metal related by $V_c + V_m = 1.$ (2)

k is the power-law index, the non-negative parameter, which can take any value between 0 and ∞, corresponding to the two extremes of completely homogenous ceramic and metal beam, respectively.

The variation of the Young's modulus along the thickness of the FGM beam is plotted in Fig. 2 with respect to various values of k.

Table 1. Some important higher-order models

Authors	Shear functions
Ambarsumyan (1958)	$f(z)=\frac{z}{2}\left(\frac{h^2}{4}-\frac{z^2}{3}\right)$
Kaczkowski (1968), Panc (1975), Reissner (1975)	$f(z)=\frac{5z}{4}\left(1-\frac{4z^2}{3h^2}\right)$
Levinson (1980), Murthy (1981), Reddy (1984)	$f(z)=z\left(1-\frac{4z^2}{3h^2}\right)$
Levy 1877, Stein (1986), Touratier (1991)	$f(z)=\frac{h}{\pi}\sin\left(\frac{\pi z}{h}\right)$
Soldatos (1992)	$f(\zeta)=h\sin\left(\frac{\zeta}{h}\right)-\zeta\cosh\left(\frac{1}{2}\right)$
Karama et al. (2003, 2009)	$f(z)=ze^{-2(z/h)^2}$
Ferreira et al. (2005)	$f(z)=\sin\left(\frac{\pi z}{h}\right)$
Aydogdu (2009)	$f(\zeta)=\zeta\alpha^{-2(\zeta/h)^2/\ln\alpha}\quad \alpha\succ 0$
Mantari et al. (2011)	$f(z)=z\alpha^{-2(z/h)^2}$
Mantari et al. (2012)	$f(\zeta)=\tan(m\zeta)$
Mantari et al. (2012)	$f(z)=\sin\left(\frac{\pi z}{h}\right)e^{m\cos(\pi z/h)}$
Mantari and Guedes-Soares (2012)	$f(z)=\sinh\left(\frac{z}{h}\right)e^{m\cosh(z/h)}$
Grover et al. (2013)	$f(z)=\sinh^{-1}\left(\frac{rz}{h}\right)-z\frac{2r}{h\sqrt{r^2+4}},\quad r=3$
Sahoo and Singh (2013)	$f(z)=\cot^{-1}\left(\frac{rh}{z}\right)-\frac{4r}{h\left(4r^2+1\right)},\quad r=0,46$

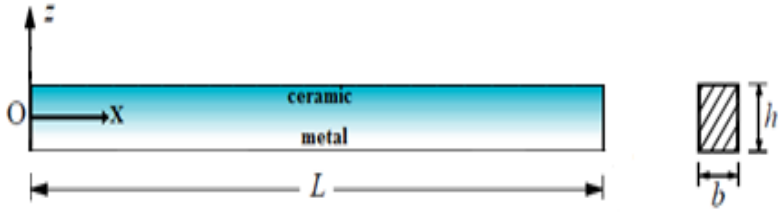

Figure (1): Schematic of a functionally graded beam

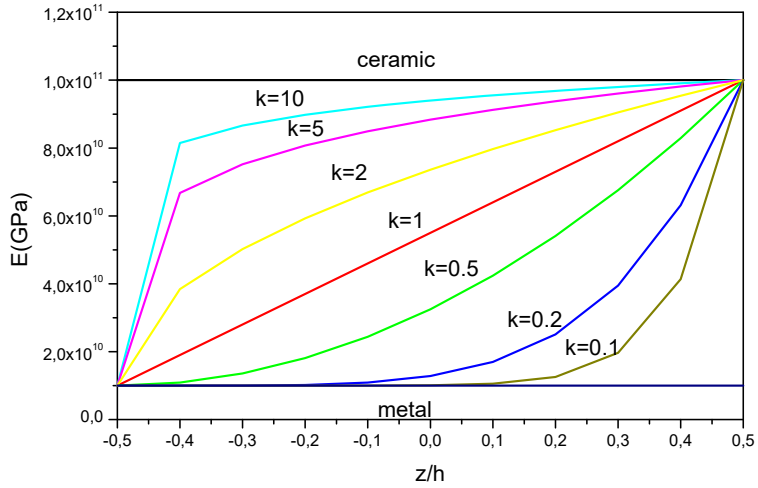

Figure (2): Variation of the Young's modulus along the thickness of the FGM beam

Position of the Neutral Surface

In order to proceed, the location of the neutral axis must be given. Due to the variation of Young's modulus through the thickness of the FGM beam, the neutral axis is no longer at the mid-plane, but it shifts from the mid-plane unless for the case of isotropic beam. Two different planes, z and z_1 are considered, as shown in Fig. 3 and Eq. (3).

$$x = x_1 \ , \ z = z_1 + h_0 \tag{3}$$

h_0 is the distance of the neutral axis from the mid-plane of the beam.

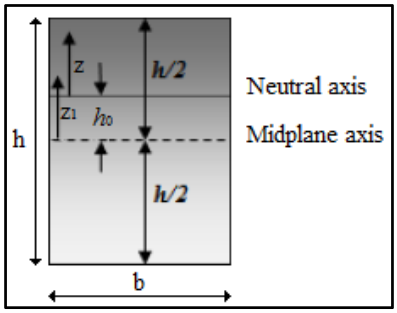

Figure (3): Position of the neutral surface

In accordance with the same procedure that was applied for Euler Bernoulli beam theory, the strain ε_x and the stress σ_x can be obtained as follows:

$$\varepsilon_x = -z_1 \frac{\partial^2 w_0}{\partial x^2} \tag{4}$$

$$\sigma_x = -z_1 E(z_1) \frac{\partial^2 w_0}{\partial x^2} \tag{5}$$

The position of the neutral surface can be given such that the total axial force at cross-section vanishes:

$$\sum F_x = 0 \rightarrow \int_{-h/2+h_0}^{+h/2+h_0} \sigma_x dA \tag{6}$$

Substituting Eq. (4) and Eq. (5) into Eq. (6) and changing the limits of integration yield:

$$b \int_{-h/2}^{+h/2} E(z) \times (z - h_0) \frac{\partial^2 w_0}{\partial x^2} dz = 0 \tag{7}$$

$$b \frac{\partial^2 w_0}{\partial x^2} \left(\int_{-h/2}^{+h/2} E(z) z dz - h_0 \int_{-h/2}^{+h/2} E(z) dz \right) = 0 \tag{8}$$

The location of the neutral axis is defined as:

$$h_0 = \frac{\hat{D}_{ab}}{\hat{D}_a} = \frac{\int_{-h/2}^{+h/2} E(z) z dz}{\int_{-h/2}^{+h/2} E(z) dz} \tag{9}$$

The elements of the reduced stiffness matrix of the FGM beam are defined by:

$$\hat{D}_a = \int_{-h/2}^{+h/2} E(z) dz = bh \left(E_m + \frac{(E_c - E_m)}{k+1} \right)$$

$$\hat{D}_{ab} = \int_{-h/2}^{+h/2} E(z) z dz = \frac{bh^2}{2} (E_c - E_m) \left(\frac{k}{(k+1)(k+2)} \right)$$

$$\hat{D}_b = \int_{-h/2}^{+h/2} E(z) z^2 dz = \frac{bh^2}{12} \left(3(E_c - E_m) \frac{k^2 + k + 2}{(k+1)(k+2)(k+3)} \right) \tag{10}$$

$\hat{D}_a$, $\hat{D}_{ab}$ and $\hat{D}_b$ are the axial, the coupling axial-bending and the bending stiffness of the beam, respectively.

Kinematics

Consider a straight beam of thickness h, composed of functionally graded material; through the thickness, material properties vary continuously and non-uniformly in the z direction (positive upward from the mid-plane) and the *xy* plane is taken to be the undeformed mid-plane of the beam (Fig. 4).

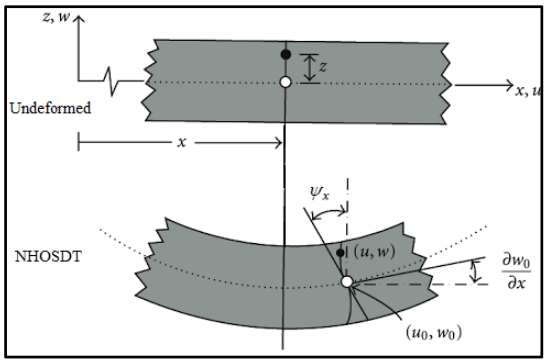

Figure (4): Kinematics of the new higher-order shear deformation theory (NHOSDT)

The assumed displacement field is as follows:

$$u(x,z) = u_0(x) - z\frac{\partial w_0}{\partial x} + f(z)\psi_x \tag{11-a}$$

$$w(x,z) = w_0(x) \tag{11-b}$$

where u_0 and w_0 are the axial and the transverse displacement of any point on the mid-plane, ψ_x is shear strain at the mid-plane of the beam.

$f(z)$ represents the shape function (NHOSDT: New Higher-Order Shear Deformation Theory) determining the distribution of the strain and the transverse shear stresses along the thickness of the beam, which can be given by this relation:

$$f(z) = z\left(\frac{h^2}{8} + \frac{9}{4}\right) - z^3\left(\frac{1}{6} + \frac{3}{h^2}\right) \tag{12-a}$$

$$f'(z) = \left(\frac{h^2}{8} + \frac{9}{4}\right) - z^2\left(\frac{1}{2} + \frac{9}{h^2}\right) \tag{12-b}$$

$$f''(z) = -z\left(1 + \frac{18}{h^2}\right) \tag{12-c}$$

The explicit expression of the displacement field can be obtained by substituting Eq. (12-a) into Eq. (11-a) as follows:

$$u(x,z) = u_0(x) - z\frac{\partial w_0}{\partial x} + \left[z\left(\frac{h^2}{8} + \frac{9}{4}\right) - z^3\left(\frac{1}{6} + \frac{3}{h^2}\right)\right]\psi_x \tag{13-a}$$

$$u(x,z) = u_0(x) - z\left[\frac{\partial w_0}{\partial x} - \left(\frac{h^2}{8} + \frac{9}{4}\right)\psi_x\right] - z^3\left(\frac{1}{6} + \frac{3}{h^2}\right)\psi_x \tag{13-b}$$

Equation (13) has the same form as those given by Levinson (1980), Murthy (1981) and Reddy (1984) for higher-order shear deformation theories:

$$u(x,z) = u_0(x) - zu_1(x) + z^2u_2(x) + z^3u_3(x) \tag{14-a}$$

The transverse shear stress is zero on the top and bottom surfaces of the beam $(z = \pm h/2)$, since the shear strain is zero. Thus, Equation (14-a) can be rewritten as:

$$u(x,z) = u_0(x) + zu_1(x) + z^3u_3(x) \tag{14-b}$$

The non-zero strains are given by:

$$\varepsilon_x(x,z) = \frac{\partial u_0}{\partial x} - z\frac{\partial^2 w_0}{\partial x^2} + f\frac{\partial \psi_x}{\partial x} = \frac{\partial u_0}{\partial x} - z\frac{\partial^2 w_0}{\partial x^2} + \left[z\left(\frac{h^2}{8} + \frac{9}{4}\right) - z^3\left(\frac{1}{6} + \frac{3}{h^2}\right)\right]\frac{\partial \psi_x}{\partial x} \tag{15-a}$$

$$\gamma_{xz}(x,z) = \frac{\partial f}{\partial z}\psi_x = \left[\left(\frac{h^2}{8} + \frac{9}{4}\right) - z^2\left(\frac{1}{2} + \frac{9}{h^2}\right)\right]\psi_x \tag{15-b}$$

$f'(z)$ equals zero at both top and bottom fibers $(z = \pm h/2)$ in order to satisfy the zero-shear stress boundary conditions at the free edges of the FGM beam.

Eq. (15) can be rewritten in matrix form as:

$$\varepsilon = \begin{Bmatrix} \varepsilon_x \\ \gamma_{xz} \end{Bmatrix} = \begin{bmatrix} 1 & -z & f & 0 \\ 0 & 0 & 0 & \dfrac{\partial f}{\partial z} \end{bmatrix} \begin{bmatrix} \dfrac{\partial u_0}{\partial x} & \dfrac{\partial w_0}{\partial x^2} & \dfrac{\partial \psi_x}{\partial x} & \psi_x \end{bmatrix}^T = S\hat{\varepsilon} \tag{15-c}$$

$\hat{\varepsilon}$ is the generalized strain vector and S is a strain-displacement transformation matrix.

The classical beam theory is recovered from the present theory when $f(z) = 0$.

The axial and shear stresses are expressed from Eq. (15) as:

$$\sigma_x = E(z)\varepsilon_x = E(z)\left(\frac{\partial u_0}{\partial x} - z\frac{\partial^2 w_0}{\partial x^2} + f\frac{\partial \psi_x}{\partial x}\right) \tag{18-a}$$

$$\tau_{xz} = G(z)\gamma_{xz} = G(z)\left(\frac{\partial f}{\partial z}\psi_x\right) \tag{18-b}$$

where b is the beam width and q is the transverse distributed force.

N, M and Q are the stress resultants defined as:

$$N = \int_{-h/2}^{h/2} \sigma_x dz \tag{21-a}$$

$$M_b = \int_{-h/2}^{h/2} z\sigma_x dz \tag{21-b}$$

$$M_s = \int_{-h/2}^{h/2} f\sigma_x dz \tag{21-c}$$

The normal strain and shear strain will be expressed in terms of transverse displacement w_0 and rotation angle θ as follows:

$$\psi_x(x) = \theta + \frac{\partial w_0}{\partial x} \tag{16}$$

By substituting Eq. (16) into Eq. (15-a) and Eq. (15-b), the strain can be written as follows:

$$\varepsilon_x(x,z) = \frac{\partial u_0}{\partial x} - z\frac{\partial^2 w_0}{\partial x^2} + \left[\left(z\left(\frac{h^2}{8}+\frac{9}{4}\right) - z^3\left(\frac{1}{6}+\frac{3}{h^2}\right)\right)\times\left(\theta + \frac{\partial w_0}{\partial x}\right)\right] \tag{17-a}$$

$$\gamma_{xz}(x,z) = \left(\left(\frac{h^2}{8}+\frac{9}{4}\right) - z^2\left(\frac{1}{2}+\frac{9}{h^2}\right)\right)\times\left(\theta + \frac{\partial w_0}{\partial x}\right) \tag{17-b}$$

or

$$\sigma = \begin{Bmatrix} \sigma_x \\ \tau_{xz} \end{Bmatrix} = \begin{bmatrix} E(z) & 0 \\ 0 & G(z) \end{bmatrix} \begin{Bmatrix} \varepsilon_x \\ \gamma_{xz} \end{Bmatrix} = D\varepsilon = DS\hat{\varepsilon} \tag{18-c}$$

Based on the principle of minimum potential energy, the governing equations and the boundary conditions will be derived as follows:

$$\delta\pi = \delta\left(U_{\text{int}} + V_{ext}\right) = 0 \tag{19}$$

The virtual strain energy U_{int} and the virtual work done by external loading V_{ext} are given respectively by:

$$\delta U_{\text{int}} = b\int_0^L \left(\int_{-h/2}^{h/2} \left(\sigma_x\delta\varepsilon_x + \tau_{xz}\delta\gamma_{xz}\right)dz\right)dx = b\int_0^L \left(N\frac{\partial\delta u_0}{\partial x} - M_b\frac{\partial^2\delta w_0}{\partial x^2} + M_s\frac{\partial\delta\psi_x}{\partial x} + Q\delta\psi_x\right)dx \tag{20-a}$$

$$\delta V_{ext} = -b\int_0^L q\delta w_0 dx \tag{20-b}$$

$$Q = \int_{-h/2}^{h/2} f'\tau_{xz} dz \tag{21-d}$$

Substituting Eq. (20-a) and Eq. (20-b) into Eq. (19), integrating by parts and setting the coefficient of the admissible displacement to zero yield:

$$\frac{\partial N}{\partial x} = 0 \tag{22-a}$$

$$\frac{\partial^2 M_b}{\partial x^2} + q = 0 \tag{22-b}$$

$$\frac{\partial^2 M_s}{\partial x^2}+\frac{\partial Q}{\partial x}+q=0 \qquad (22\text{-c})$$

Under the following boundary conditions:

$$u \quad \text{or} \quad N \qquad (23\text{-a})$$

$$w_0 \quad \text{or} \quad Q_b=\frac{\partial M_b}{\partial x} \qquad (23\text{-b})$$

$$\psi_x \quad \text{or} \quad Q_s=\frac{\partial M_s}{\partial x}+Q \qquad (23\text{-c})$$

$$\frac{\partial w_0}{\partial x} \quad \text{or} \quad M_b \qquad (23\text{-d})$$

$$\frac{\partial w_0}{\partial x} \quad \text{or} \quad M_s \qquad (23\text{-e})$$

NUMERICAL RESULTS AND DISCUSSION

In this section, various numerical examples are carried out and discussed in order to demonstrate the efficiency of the proposed theory in predicting the bending responses of FGM beams under distributed load. Different boundary conditions (BCs) are considered. The results are displayed later in graphical form to compare them with the data available in the literature and to figure out the effects of different material distributions, slenderness ratios, boundary conditions and neutral axis on the static characteristics of FGM beams.

The non-dimensional quantities used in the present analysis are defined as:

$$\frac{E_c}{E_m}=10,\ \bar{w}=100\frac{E_m h^3}{qL^4}w\left(\frac{L}{2}\right),\ \bar{\sigma}_{xx}=\frac{h}{qL}\sigma_x\left(\frac{L}{2},\frac{h}{2}\right),\ \bar{\sigma}_{xz}=\frac{h}{qL}\sigma_{xz}\left(0,0\right) \qquad (24)$$

Max. Deflection

The maximum deflections of thick/thin FGM beams due to uniformly distributed load for different boundary conditions (BCs) are presented in the first sub-section. For a constant power-law index and identical L/h, the values of the non-dimensional maximum deflection with C-F FGM beam are higher than those for the other boundary conditions (S-S and C-C); this is due to the fact that a change in the boundary conditions reflects a change in the beam's rigidity. In other words, as the rigidity of the structure increases, the deflection decreases.

Simply-Supported (S-S) BCs

The non-dimensional maximum deflection of thick/thin (S-S) FGM beam due to uniform distributed load is shown in Figs. 5-6. As seen from the figures, increasing the power-law index tends to increase the deflections and this is due to the fact that an increase in power-law index results in a decrease in the value of elasticity modulus and hence makes FGM beams more flexible. The deflection is proportional with power-law index. It can be also noted that the deflections of short beams are higher than those of slender beams. It is interesting to note also that the maximum value of deflection occurs at the middle of the beam.

Clamped-Clamped (C-C) BCs

Figures 7 and 8 illustrate the non-dimensional maximum deflection of (C-C) FGM beam for various values of power-law index in case of thick beam and thin beam, respectively. As illustrated, increasing the power-law index leads to an increase in the deflections. Similar to S-S counterparts, the deflections of smaller values of L/h are higher than those of slender beams. It is worth noting also that the maximum value of deflection occurs at the beam center.

Clamped-Free (C-F) BCs

Figures 9 and 10 highlight the effect of power-law index on the non-dimensional maximum deflection of cantilever (C-F) FGM beam. It is seen that when the power-law index increases, deflections show a downward trend. Minimum deflection values are obtained for full ceramic beams (k=0). The deflections with lower L/h ratio are more strongly affected by the power-law index than those with higher L/h ratio. The maximum value of deflection occurs at the free end of the beam.

Normal Stress

The normal stress distributions for different boundary conditions (BCs) and different length-to-thickness ratios are depicted in the second section (Fig.11-Fig.16).

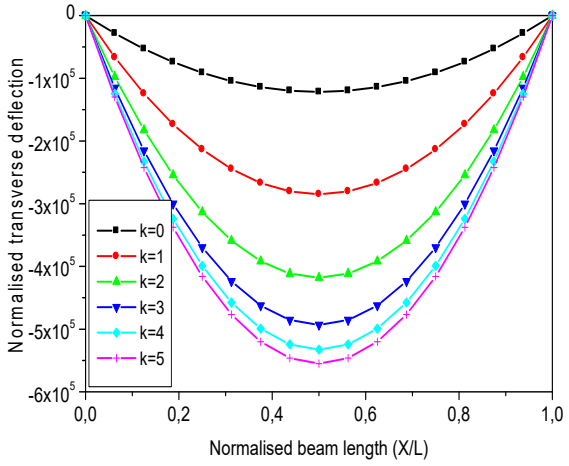

Figure (5): Non-dimensional maximum deflection of FGM beam for L/h=5 (S-S)

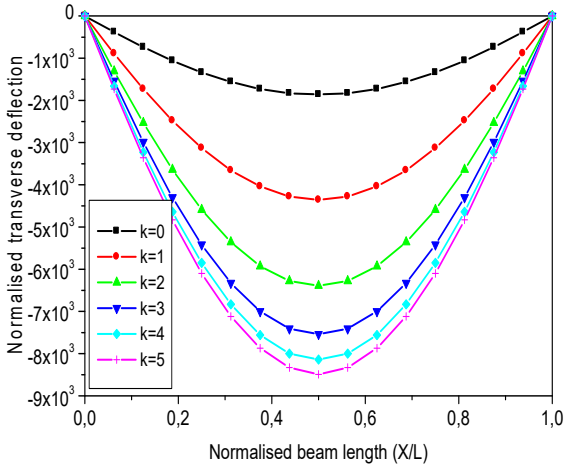

Figure (6): Non-dimensional maximum deflection of FGM beam for L/h=100 (S-S)

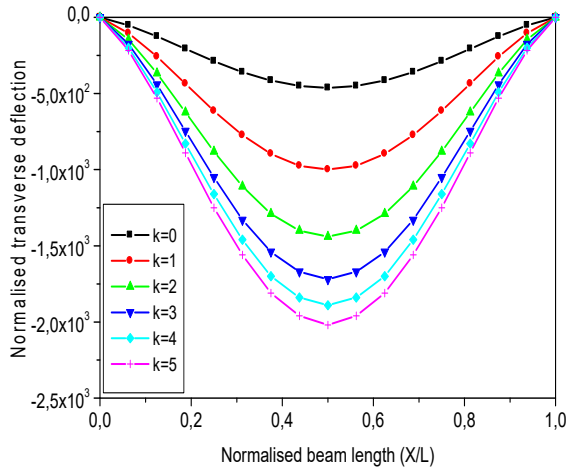

Figure (7): Non-dimensional maximum deflection of FGM beam for L/h=5 (C-C)

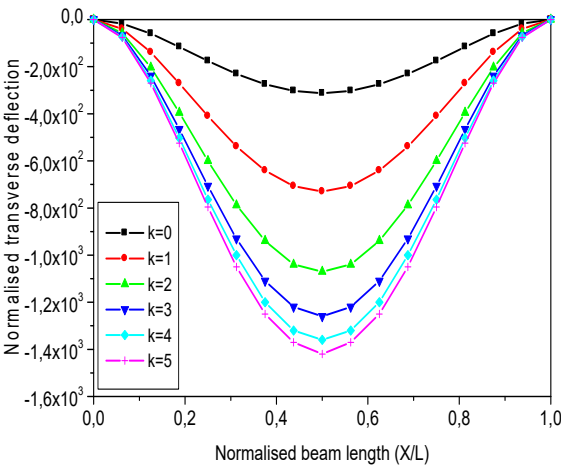

Figure (8): Non-dimensional maximum deflection of FGM beam for L/h=100 (C-C)

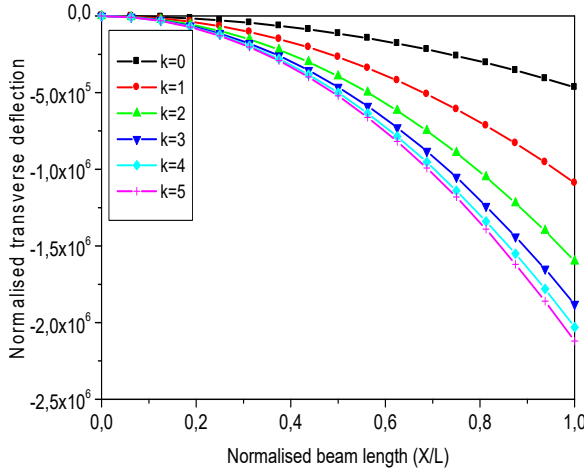

Figure (9): Non-dimensional maximum deflection of FGM beam for L/h=5 (C-F)

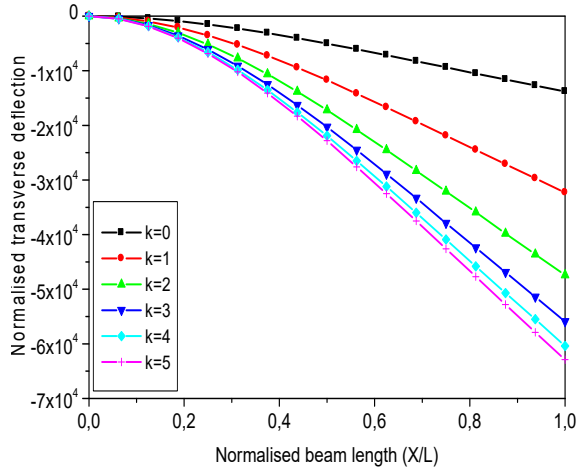

Figure (10): Non-dimensional maximum deflection of FGM beam for L/h=100 (C-F)

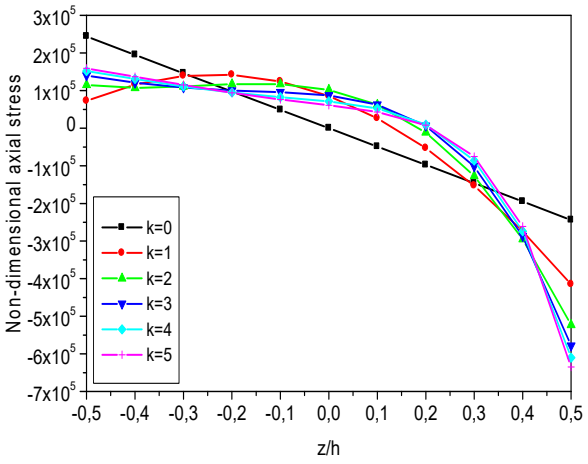

Figure (11): Non-dimensional normal stress at x = L/2 of FGM beam for L/h=5 (S-S)

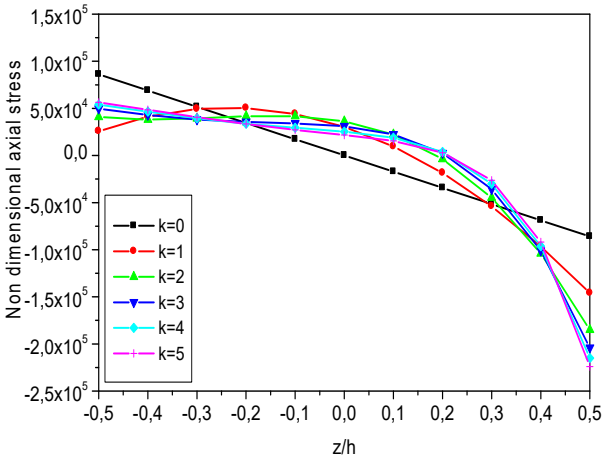

Figure (12): Non-dimensional normal stress at x = L/2 of FGM beam for L/h=100 (S-S)

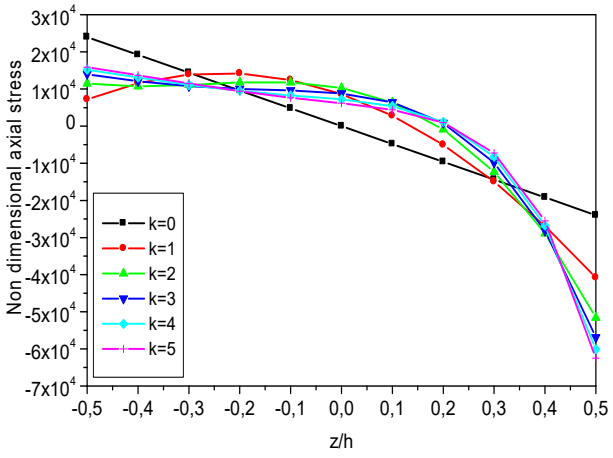

Figure (13): Non-dimensional normal stress at x = L/2 of FGM beam for L/h=5 (C-C)

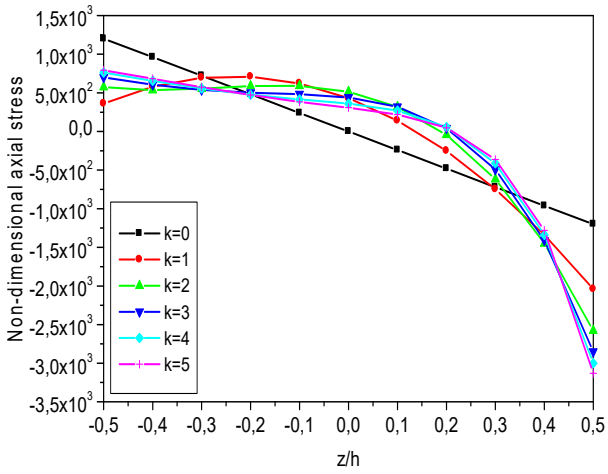

Figure (14): Non-dimensional normal stress at x = L/2 of FGM beam for L/h=100 (C-C)

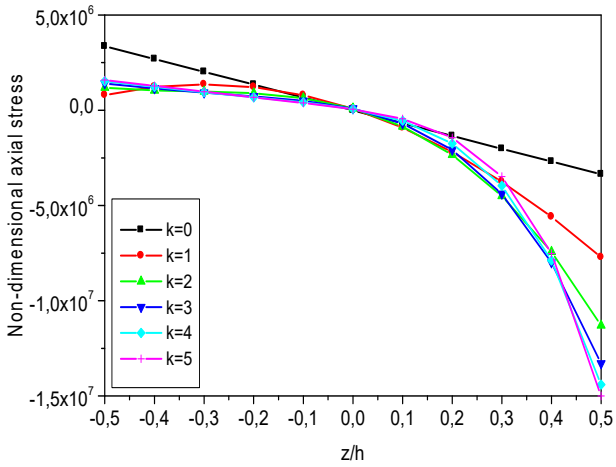

Figure (15): Non-dimensional normal stress at x = L/2 of FGM beam for L/h=5 (C-F)

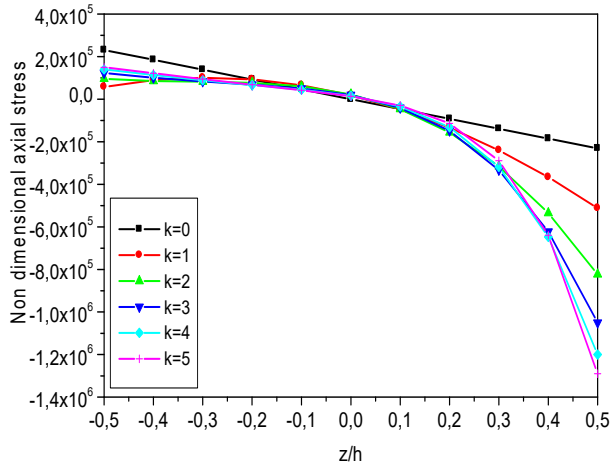

Figure (16): Non-dimensional normal stress at x = L/2 of FGM beam for L/h=100 (C-F)

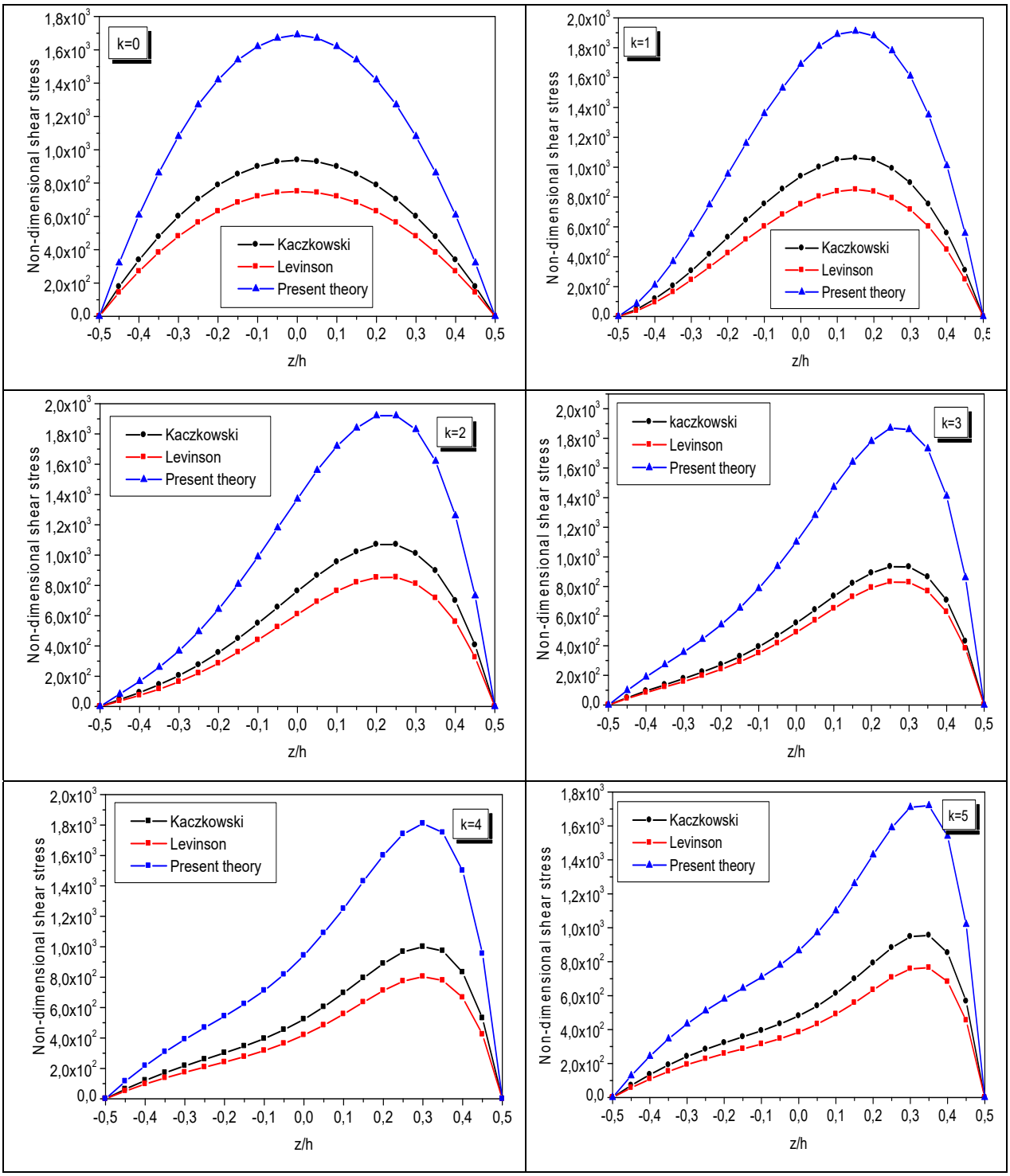

Figure (17): Non-dimensional shear stress at x = 0 of FGM beam for L/h=5 (S-S/C-C)

It can be seen that the normal stress distribution is linear for full ceramic beam. Additionally, the values of tensile and compressive stresses for isotropic beam are equal. For other values of k, the normal stress distribution is not linear; the values of compressive stresses are greater than tensile stresses. Furthermore, the value of normal stress is zero at the mid-plane, but it is clearly visible that these values are not zero at the mid-plane of the FGM beam for the other values of k, which confirms that the neutral plane moves towards the upper side of the FGM beam and this is due to the variation of the modulus of elasticity through the thickness of the beam.

It is important to note that the values of normal stress for L/h=100 are higher than those for L/h=5. Moreover, for identical L/h and for a constant power-law index, the non-dimensional normal stresses with C-F end conditions are higher than those for the other boundary conditions (S-S and C-C).

Shear Stress

The last section is devoted mainly to show the variation of the shear stress across the thickness of the FGM beam for different length-to-thickness ratios, boundary conditions and for different higher-order shear deformation theories at x=0, (Fig. 17-Fig. 20).

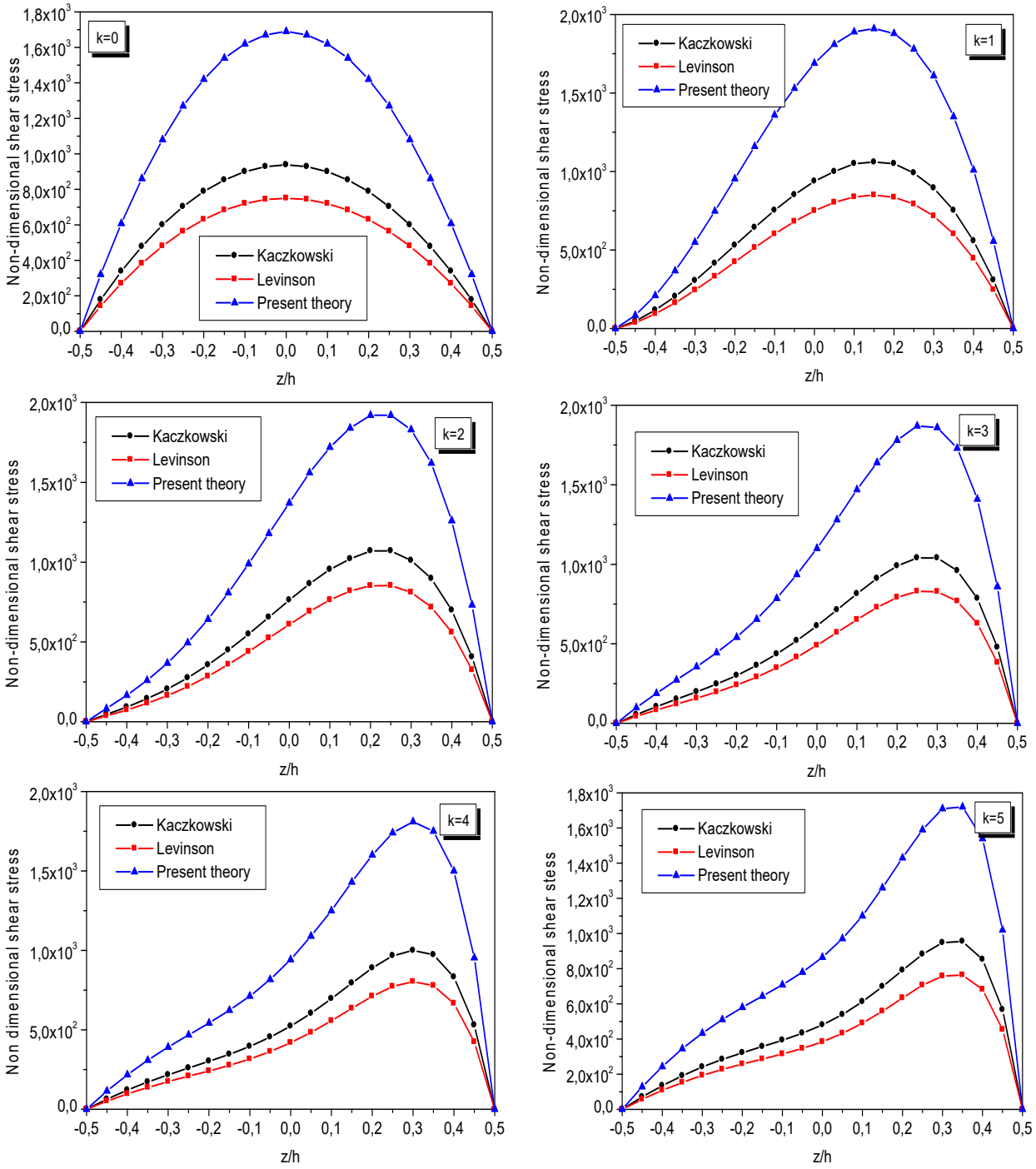

Figure (18): Non-dimensional shear stress at x = 0 of FGM beam for L/h=100 (S-S/C-C)

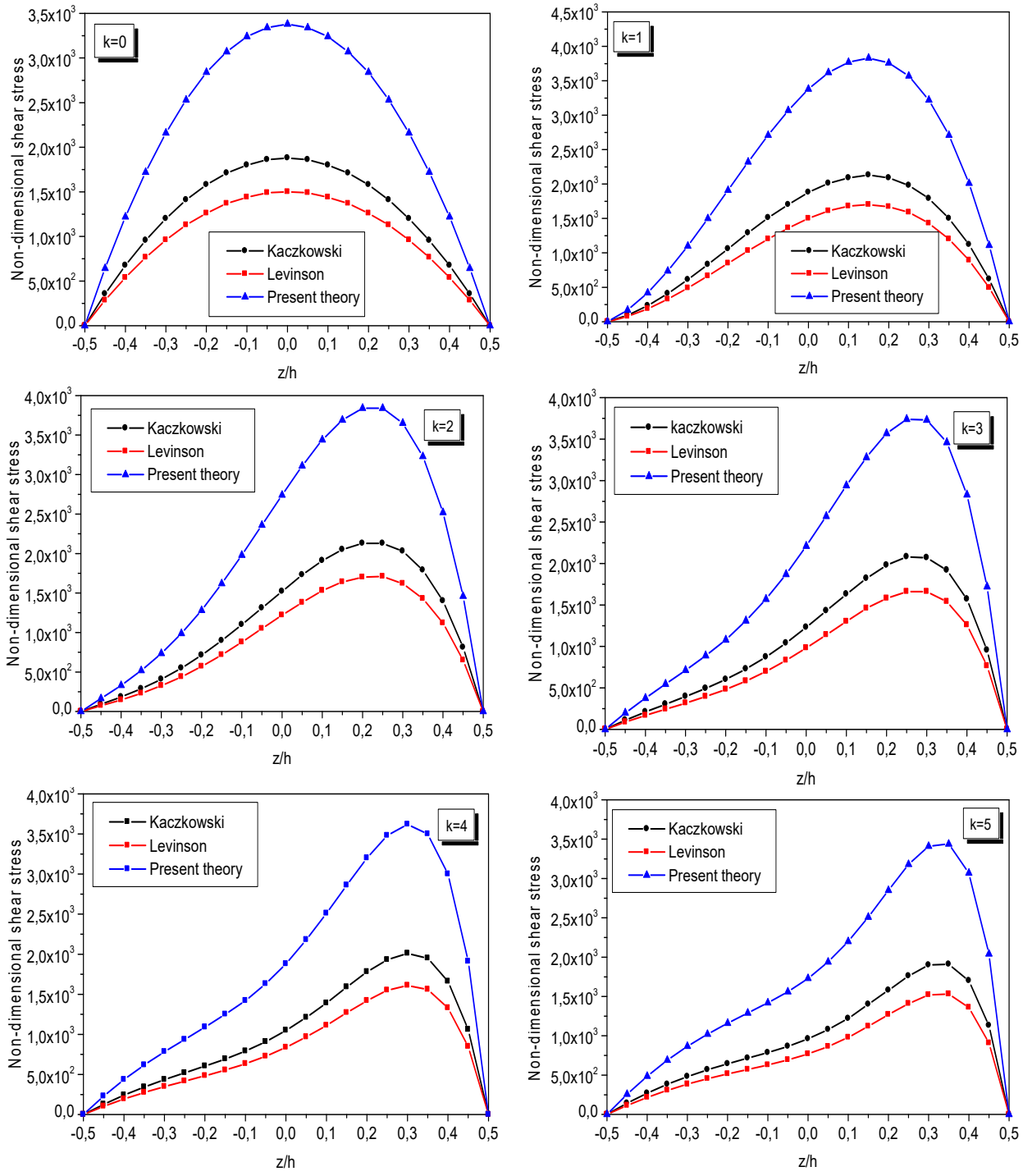

Figure (19): Non-dimensional shear stress at x = 0 of FGM beam for L/h=5 (C-F)

It can be observed that the curves obtained using the present theory follow the same pathway as those given by other beam theories (Kaczkowski and Levinson) for all values of power-law index k and length-to-thickness ratio L/h. This is related to the different transverse shear strain shape functions used by each author. It is interesting to note also that the maximum value of shear stress occurs at the neutral axis and not at the mid-plane unless for a beam with symmetrical Young's modulus (full ceramic beam), which confirms that the neutral axis for FGM beam shifts towards ceramic-rich surface and its position increases with the increase of k.

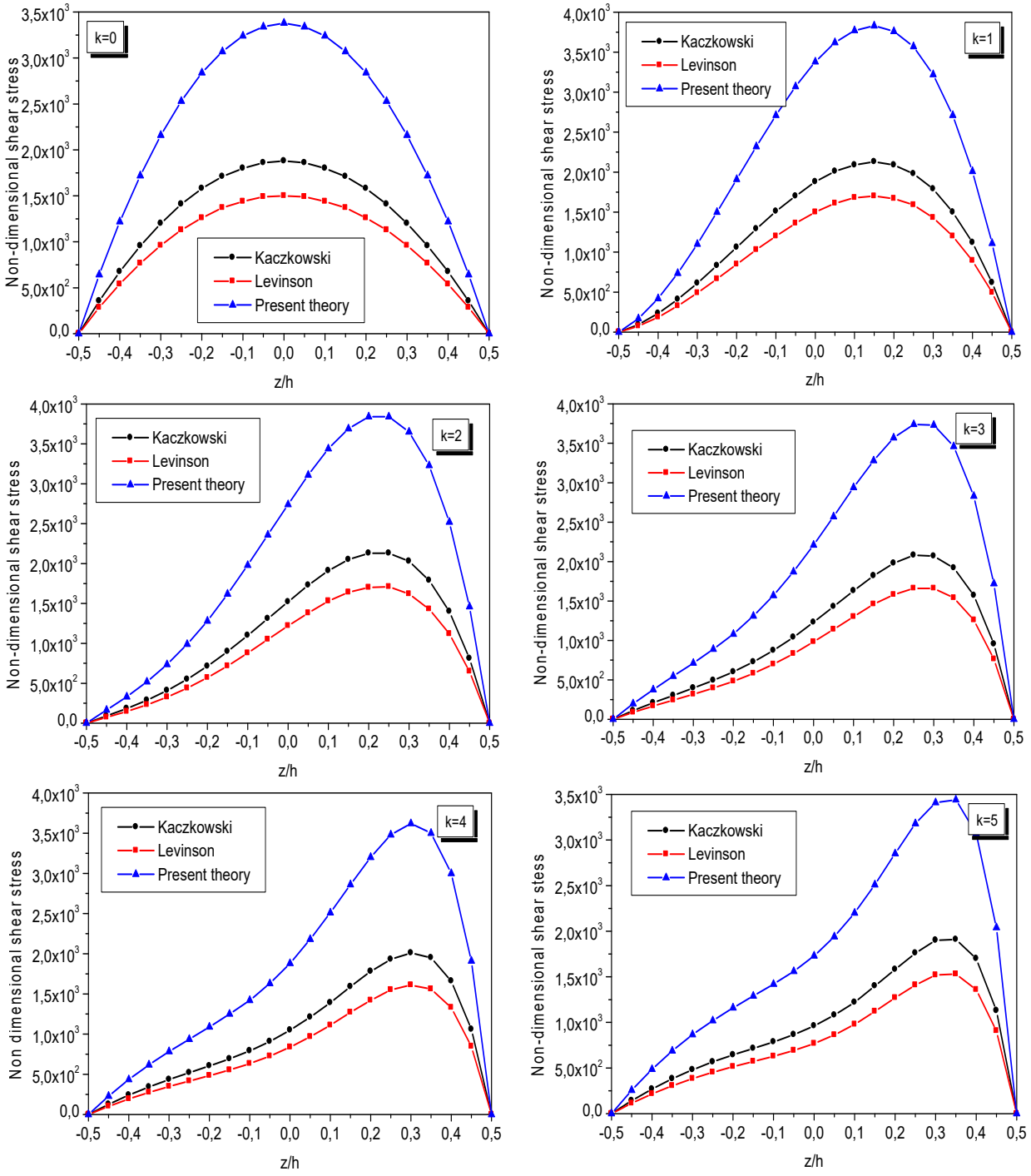

Figure (20): Non-dimensional shear stress at x = 0 of FGM beam for L/h=100 (C-F)

The values of shear stress for L/h=100 are higher than those for L/h=5 for all boundary conditions. The most important observation is that for a constant power-law index and identical L/h, the shear stress values are similar for S-S and C-C FGM beams. Furthermore, the values of the shear stress with C-F beams are higher than those with S-S and C-C counterparts.

It can be deduced that, in the case of transverse shear stress, all shear deformation beam theories give different results. It can be explained by the different shape functions determining the distribution of the strain and the transverse shear stresses used in each model.

CONCLUSIONS

The present manuscript tries to introduce a complete study for static analysis of FGM beams, using a new higher-order shear deformation theory. Numerical solutions are derived in detail for all boundary conditions, as they have not been presented elsewhere. Impacts of material distribution, boundary conditions, aspect ratio and neutral axis on the mid-plane deflection, normal stress and shear stress are presented and figured out.

The main conclusions reached by the above study can be summarized as:

1. Increasing the power-law index tends to increase the deflections. This is due to the fact that an increase in power-law index results in a decrease in the value of elasticity modulus and hence makes FGM beams more flexible. So, the deflection is proportional with power-law index.
2. For a constant power-law index and identical L/h, the values of the non-dimensional maximum deflection with C-F FGM beams are higher than those for the other boundary conditions (S-S and C-C), which is due to the fact that a change in the boundary conditions results in a change in the beam stiffness. In other words, as the rigidity of the structure increases, the deflection decreases.
3. The deflections of short beams are higher than those of slender beams. Furthermore, the maximum value of deflection occurs at the middle of the beam for S-S and C-C end conditions and at the free end for C-F counterpart.
4. The normal stress distribution is linear for full ceramic beam and the values of tensile and compressive stresses are equal for isotropic beam. For other values of k, the normal stress distribution is not linear and the values of compressive stresses are higher than tensile stresses. Furthermore, the value of normal stress is zero at the mid-plane, but it is clearly visible that these values are not zero at the mid-plane of the FGM beam for the other values of k, which confirms that the neutral plane moves towards the upper side of the FGM beam and this is due to the variation of the modulus of elasticity through the thickness of the FGM beam.
5. The values of normal and shear stresses for L/h=100 are higher than those for L/h=5. Moreover, for identical L/h and for a constant power-law index, the non-dimensional normal stresses with C-F end conditions are higher than those for the other boundary conditions (S-S and C-C).
6. The maximum value of shear stress occurs at the neutral axis and not at the mid-plane unless for a beam with symmetrical Young's modulus. The neutral axis for FGM beam shifts towards ceramic-rich surface and the distance between neutral axis and mid-plane axis increases with the increase of k.
7. For a constant power-law index and identical L/h, the shear stress values are similar for S-S and C-C FGM beams.
8. It can be deduced that in the case of transverse shear stress, all shear deformation beam theories give different results. This can be explained by the different shape functions determining the distribution of the strain and the transverse shear stresses used in each model.
9. It is believed that the presented theory will provide a reference which other researchers can use for their studies.

REFERENCES

Ambarsumyan, S. (1958). "K tieorii izgiba anisotropnvch plasinok". Izv. Akad. Nauk. SSR, 5, 69-77.

Aydogdu, M. (2009). "A new shear deformation theory for laminated composite plates". Composite Structures, 89 (1), 94-101.

Bouazza, M., Amara, K., and Benseddiq, N. (2017). "Mechanical buckling analysis of functionally graded plates using a new refined theory". Jordan Journal of Civil Engineering, 11 (1), 64-79.

Chakraborty, A., Gopalakrishnan, S., and Reddy, J.N. (2003). "A new beam finite element for the analysis of functionally graded materials". International Journal of Mechanical Sciences, 45 (3), 519-539.

Ferreira, A., Roque C., and Jorge, R. (2005). "Analysis of composite plates by trigonometric shear deformation theory and multiquadrics". Computers & Structures, 83 (27), 2225-2237.

Grover, N., Maiti, D., and Singh, B. (2013). "A new inverse hyperbolic shear deformation theory for static and buckling analysis of laminated composite and sandwich plates". Composites Structures, 95, 667-675.

Kaczkowski, Z. (1968). "Plates: Statical calculations". Arkady, Warsaw.

Kadoli, R., Akhtar, K., and Ganesan, N. (2008). "Static analysis of functionally graded beams using higher-order shear deformation theory". Applied Mathematical Modeling, 32 (12), 2509-2525.

Karama, M., Afaq, K., and Mistou, S. (2003). "Mechanical behaviour of laminated composite beam by the new multi-layered laminated composite structures model with transverse shear stress continuity". International Journal of Solids and Structures, 40 (6), 1525-1546.

Karama, M., Afaq K., and Mistou S. (2009). "A new theory for laminated composite plates". Proceedings of the Institution of Mechanical Engineers- Part L*:* Journal of Materials: Design and Applications, 223 (2), 53-62.

Levinson, M. (1980). "An accurate, simple theory of the statics and dynamics of elastic plates". Mechanics Research Communications, 7 (6), 343-350.

Levy, M. (1877). "Mémoire sur la théorie des plaques élastiques planes". Journal de Mathématiques Pures et Appliquées, 219-306.

Mantari, J., Oktem A., and Guedes-Soares, C. (2011). "Static and dynamic analysis of laminated composite and sandwich plates and shells by using a new higher-order shear deformation theory". Composite Structures, 94 (1), 37-49.

Mantari, J., Oktem, A., and Guedes-Soares, C. (2012). "A new trigonometric shear deformation theory for isotropic, laminated composite and sandwich plates". International Journal of Solids and Structures, 49 (1), 43-53.

Mantari, J., Oktem A., and Guedes-Soares, C. (2012). "A new higher-order shear deformation theory for sandwich and composite laminated plates". Composites-Part B: Engineering, 43 (3), 1489-1499.

Mantari, J., and Guedes-Soares, C. (2012). "Analysis of isotropic and multilayered plates and shells by using a generalized higher-order shear deformation theory". Composite Structures, 94 (8), 2640-2656.

Meksi, A., Belakhdar, K., Bouguenina, O., Tounsi, A., and Bedia El-Abbes, Adda. (2018). "Effect of parabolic-concave thickness variation on the mechanical buckling resistance of simply supported FGM plates". Jordan Journal of Civil Engineering, 12 (2), 216-227.

Murthy, M. (1981). "An improved transverse shear deformation theory for laminated antisotropic plates". NASA Technical, 1-37.

Nguyen Trung-Kien, Nguyen T. Truong-Phong, Vo Thuc, P., and Thai Huu-Tai. (2015). "Vibration and buckling analysis of functionally graded sandwich beams by a new higher-order shear deformation theory". Composites-Part B: Engineering, 76, 273-285.

Panc, V. (1975). "Theories of elastic plates". Prague: Academia: Springer.

Pindera, M.-J., and Dunn, P. (1995). "An evaluation of coupled microstructural approach for the analysis of functionally graded composites *via* the finite element method". NASA CR 195455. Lewis Research Center, Cleveland, OH.

Reddy, J.N. (1984). "A simple higher-order theory for laminated composite plates". Journal of Applied Mechanics, 51 (4), 745-752.

Reissner, E. (1975). "On transverse bending of plates, including the effect of transverse shear deformation". International Journal of Solids and Structures, 11 (5), 569-573.

Rezaiee-Pajand, M., and Masoodi Amir, R. (2016). "Exact natural frequencies and buckling load of functionally graded material-tapered beam-columns considering semi-rigid connections". Journal of Vibration and Control, 24 (9), 1787-1808.

Rezaiee-Pajand, M., Masoodi, Amir, R., and Mokhtari, M. (2018). "Static analysis of functionally graded non-prismatic sandwich beams". Advances in Computational Design, 3 (2), 165-190.

Sahoo, R., and Singh, B. (2013). "A new shear deformation theory for the static analysis of laminated composite and sandwich plates". International Journal of Mechanical Sciences, 75, 324-336.

Sankar, B.V. (2001). "An elasticity solution for functionally graded beams". Composites Science and Technology, 61, 689-696.

Soldatos, K.P. (1992). "A transverse shear deformation theory for homogeneous monoclinic plates". Acta Mechanica, 94 (3-4), 195-220.

Stein, M. (1986). “Nonlinear theory for plates and shells including the effects of transverse shearing”. AIAA Journal, 24 (9), 1537-1544.

Thai Huu-Tai, and Vo Thuc, P. (2012). “Bending and free vibration of functionally graded beams using various higher-order shear deformation beam theories”. International Journal of Mechanical Sciences, 62 (1), 57-66.

Thai Huu-Tai, and Vo Thuc, P. (2012). “A nonlocal sinusoidal shear deformation beam theory with application to bending, buckling and vibration of nanobeams”. International Journal of Engineering Science, 54, 58-66.

Touratier, M. (1991). “An efficient standard plate theory”. International Journal of Engineering Science, 29 (8), 901-916.

Vo Thuc, P., Thai Huu-Tai, Nguyen Trung-Kien, Maheri Alireza, and Lee Jaehong. (2014). “Finite element model for vibration and buckling of functionally graded sandwich beams based on a refined shear deformation theory”. Engineering Structures, 64, 12-22.

Vo Thuc, P., and Thai Huu-Tai, (2012). “Static behavior of composite beams using various refined shear deformation theories”. Composite Structures, 94 (8), 2513-2522.

Ziou, H., Guenfoud, H., and Guenfoud, M. (2020). “Buckling analysis behavior of functionally graded beams”. Jordan Journal of Civil Engineering, 14 (3), 347-358.

Ziou, H., Himeur, M., Guenfoud, H., and Guenfoud, M. (2020). “An efficient finite element formulation based on deformation approach for bending of functionally graded beams”. Journal of Solid Mechanics, 12 (2), 343-357.

Ziou, H., Guenfoud, H., and Guenfoud, M. (2016). “Numerical modeling of a Timoshenko FGM beam using the finite element method”. International Journal of Structural Engineering, 7 (2), 239-261.